Mon. Not. R. Astron. Soc. **330,** 1034–1040 (2002)

ISO-LWS two-colour diagram of young stellar objects

S. Pezzuto,[1★] F. Grillo,[1] M. Benedettini,[1] E. Caux,[2] A. M. Di Giorgio,[1] T. Giannini,[3] S. J. Leeks,[4,5] D. Lorenzetti,[3] B. Nisini,[3] P. Saraceno,[1] L. Spinoglio[1] and E. Tommasi[6]

[1]*Istituto di Fisica dello Spazio Interplanetario, CNR, Via Fosso del Cavaliere 100, 00133 Roma, Italy*
[2]*CESR, BP 4346, 31028 Toulouse Cedex 04, France*
[3]*Osservatorio di Roma, Via Frascati 33, 00040 Monte Porzio, Italy*
[4]*Queen Mary & Westfield College, University of London, Mile End Road, London E1 4NS*
[5]*Department of Physics & Astronomy, Cardiff University, PO Box 913, Cardiff CF24 3YB*
[6]*Agenzia Spaziale Italiana, Viale Liegi 26, 00198 Roma, Italy*

Accepted 2001 November 12. Received 2001 November 12; in original form 2001 June 5

ABSTRACT

We present a [60–100] versus [100–170]μm two-colour diagram for a sample of 61 young stellar objects (YSOs) observed with the Long Wavelength Spectrometer (LWS) on-board the *Infrared Space Observatory* (*ISO*). The sample consists of 17 Class 0 sources, 15 Class I, nine Bright Class I ($L_{\rm bol} > 10^4\,{\rm L}_\odot$) and 20 Class II (14 Herbig Ae/Be stars and six T Tauri stars). We find that each class occupies a well-defined region in our diagram with colour temperatures increasing from Class 0 to Class II. Therefore the [60–100] versus [100–170] two-colour diagram is a powerful and simple tool to derive from future (e.g. with the *Herschel Space Observatory*) photometric surveys the evolutionary status of YSOs. The advantage over other tools already developed is that photometry at other wavelengths is not required: three flux measurements are enough to derive the evolutionary status of a source. As an example we use the colours of the YSO IRAS 18148−0440 to classify it as Class I. The main limitation of this work is the low spatial resolution of the LWS which, for some objects, causes a high uncertainty in the measured fluxes due to background emission or to source confusion inside the LWS beam.

Key words: circumstellar matter – stars: formation – stars: fundamental parameters – stars: pre-main-sequence.

1 INTRODUCTION

It is generally accepted that the evolutionary status of young stellar objects (YSOs) is characterized by the shape of their spectral energy distribution (SED). During the early phases of star formation the emitted SED has the shape of a cold, few-tens-of-K, blackbody modified by the emissivity of the dust. The central object, even when already formed, is not visible at any wavelength since the surrounding dust envelope completely obscures the inner region. As the evolution goes on, the optical depth of the dust decreases making the central object optically visible until its spectrum looks like that of a normal star with an infrared excess due to the residual circumstellar material. It is thus clear that the characterization of the evolutionary status of YSOs is better done by observing dust emission rather than stellar radiation, which is only visible during the late phases of star formation.

The *Infrared Space Observatory* (*ISO*) (Kessler et al. 1996) has opened a new observing window covering the near to far-infrared (FIR) wavelengths up to $\lambda \sim 200\,\mu$m, where the dust emission peaks. It is then natural to use *ISO* data to derive the evolutionary status of YSOs. To this aim we introduce a two-colour diagram defined between 60 and 170 μm which exploits almost all the spectral coverage of the Long Wavelength Spectrometer (LWS) (Clegg et al. 1996). Already with *IRAS* data two-colour diagrams have been used to infer the evolutionary phase of YSOs (e.g. Beichman et al. 1986, or Berrilli et al. 1989); however, the LWS extends the far-infrared spectral coverage of *IRAS* by a factor ∼2 in the region where the peaks of emission of blackbodies with temperatures in the range 15–30 K fall, typical of YSOs in the early phases of their evolution.

Tommasi & Pezzuto (1997) and Pezzuto et al. (1999) have indeed already shown that such a diagram allows one to identify the evolutionary status of YSOs. While in previous work a small sample of objects was used, we have now completed an analysis of the whole sample of YSOs observed by the LWS as part of the core program dedicated to the study of star formation.

With respect to previous evolutionary diagnostic tools, like the spectral index α (Adams, Lada & Shu 1987), the bolometric

★E-mail: pezzuto@ifsi.rm.cnr.it

Table 1. The sample of YSOs observed. Sources have been grouped according to their known evolutionary status. Inside each group sources have been sorted in increasing right ascension. An asterisk flags objects classified as FU Orionis. The [60–100] *IRAS* colour has been computed by using the fluxes reported in the SIMBAD data base or the fluxes given in the quoted reference. The *IRAS* colour of L 1448 N has been obtained by adding the fluxes of L 1448 N and L 1448 NW, which fall inside the LWS beam.

	IRAS ID	[60–100] LWS	[60–100] *IRAS*	[100–170]		*IRAS* ID	[60–100] LWS	[60–100] *IRAS*	[100–170]
Class 0					**Bright Class I**				
L 1448 N		0.53	0.54[1]	0.20	NGC 281 W	00494+5617	0.39	0.38[8]	0.025
L 1448 mm		0.53		0.094	AFGL 437	03035+5819	0.0096	0.089	−0.19
NGC 1333 *IRAS* 2	03258+3104	0.30	0.46[2]	−0.077	AFGL 490	03236+5836	0.025	0.039	−0.12
NGC 1333 *IRAS* 6		0.50	0.52[2]	0.38	NGC 2024 IRS2		−0.11		−0.23
NGC 1333 *IRAS* 4		0.84	0.68[2]	0.22	NGC 6334 I		0.14		−0.13
	03282+3035	0.57	0.77	0.28	W 28 A2		−0.0016		−0.24
VLA 1		0.54		0.24	M 8 E		0.19		−0.11
NGC 2024 FIR 3		0.00		−0.20	GGD 27 IRS		−0.0084		−0.20
NGC 2024 FIR 5		−0.078		−0.21	S 87 IRS 1	19442+2428	0.025	0.18[9]	−0.12
HH 25 mm		0.57		0.19					
HH 24 mm		0.47		0.23	**Herbig Ae/Be**				
VLA 1623		0.52		0.20	LK Hα 198	00087+5833	0.21	0.17[10]	−0.037
	16293−2422	0.55	0.61	0.12	V376 Cas		0.067	0.16[10]	−0.086
L483	18148−0440	0.39	0.27	0.063	*Z CMa	07013−1128	0.091	0.041	−0.091
Serpens FIRS 1	18273+0113	0.53	0.41[3]	0.081	HD 97048	11066−7722	0.11	0.048	−0.014
B 335	19345+0727	0.69	0.70	0.19	DK Cha	12496−7650	−0.0026	−0.082	−0.032
L 723	19156+1906	0.58	0.48	0.20	CoD −39° 8581	13547−3944	0.54	0.62[11]	0.10
					CoD −42° 11721	16555−4237	0.087	0.062	−0.013
Class I					MWC 297	18250−0351	−0.062	0.30	−0.27
SVS 13	03259+3105	0.26	0.39[2]	0.028	R CrA	18585−3701	0.27	0.30	−0.060
*L 1551 IRS 5	04287+1801	0.15	0.089	−0.043	T CrA		0.43		0.26
L1641 N	05338−0624	0.40	0.38	0.12	PV Cep	20453+6746	0.12	0.064	0.0023
HH 26 IRS		0.28		0.27	V645 Cyg	21381+5000	0.098	0.089	−0.084
HH 46 IRS	08242−5050	0.34	0.35	0.089	LK Hα 234	21418+6552	0.16	0.25	−0.14
WL 16		0.23		0.071	MWC 1080	23152+6034	0.21	0.46	−0.094
Elias 29		0.21	0.41[4]	0.098					
ρ Oph IRS 43		0.30		0.26	**T Tauri**				
ρ Oph IRS 44		0.26		0.24	*RNO 1B		0.34		0.016
Re 13	16289−4449	0.26	0.53[5]	0.13	T Tau	04190+1924	0.071	−0.0026	−0.12
*HH 57 IRS	16289−4449	0.17	−0.054[5]	0.071	DG Tau	04240+2559	0.071	0.070	0.059
L 379 IRS 3	18265−1517	0.39	0.46[6]	0.088	HL Tau	04287+1807	0.055	<0.77	−0.057
IC 1396 N		0.41		0.11	SR 9		0.53		0.18
NGC 7129 FIRS 2		0.36	0.33[7]	0.077	*Elias 1–12	21454+4718	0.40	0.32	0.18
L 1206	22272+6358	0.21	0.28	−0.10					

Notes to the table: [1]Barsony et al. (1998); [2]Jennings et al. (1987) (actually [50–100]); [3]Hurt & Barsony (1996); [4]Young et al. (1986); [5]Prusti et al. (1993); [6]Hilton et al. (1986); [7]Eiroa et al. (1998); [8]Mookerjea et al. (2000); [9]Chini et al. (1986); [10] Hillenbrand et al. (1992); [11]White (1993).

temperature (Myers & Ladd 1993; Chen et al. 1995), and the $L_{\rm bol}$ versus $F_{1.3{\rm mm}}$ diagram (Saraceno et al. 1996), our method can be applied to YSOs in all evolutionary phases (Class 0, I and II objects), and does not require the knowledge of either $L_{\rm bol}$, or the complete SED.

In Section 2 we present the sample, and the data analysis is briefly reported; in Section 3 the two-colour diagram is shown and discussed; the conclusions are summarized in Section 4.

2 OBSERVATIONS AND DATA REDUCTION

Our sample consists of 61 YSOs for which an LWS full range grating spectrum, 43–197 μm with a resolution $\lambda/\Delta\lambda \sim 200$, was obtained. It corresponds to almost all the observations carried out with the LWS as part of the *ISO*-LWS core programme on star formation, excluding a few sources whose spectra are too noisy to derive reliable photometric data. We have decided to include for this paper only the sample of our guaranteed time, to have a homogeneous set of data taken with the same observational procedure and comparable integration times. Our original sample, to which the 61 objects discussed here belong, was selected on the basis of the knowledge of the instrument (spatial and spectral resolution, sensitivity) and on the spectral characteristics of the known sources, at the time of the definition of the observing programmes (around 1995).

The raw data have been processed with version 8 of the off-line pipeline[1] and analysed with the ISAP package. After removing bad points, the scans were averaged. The strong source correction, which takes into account the non-linearity of the detectors at high fluxes (Leeks et al. 1999; Leeks 2000), was applied to the data where necessary.

The LWS spectra are affected by instrumental effects (fringes, memory effects, bad flat field and dark current removal, see Gry et al. 2001), which might potentially influence the shape of the spectrum. Such effects can be, at least partially, corrected by using specific routines (LIA, the LWS Interactive Analysis). However, it has been verified (Grillo 2001) that for the majority of our objects the fluxes are not considerably changed by applying these routines. In the end, we adopted the fluxes computed without any correction.

[1] After submitting the manuscript, the final version of this software has been released (version 10). The changes in the data processing with respect to version 8 are not relevant to the present work, as we verified for some faint or noisy sources (for instance SR 9).

For some objects, one or more off-source positions have been observed to estimate the background emission. In our previous work (Pezzuto et al. 1999) we compared the colours before and after removing the background and we found that, again in a statistical sense, the subtraction does not alter our results. Moreover, in star-forming regions the presence of a diffuse, not homogeneous, cloud emission makes it difficult to define the background level. In addition, when the instrument does not have enough spatial resolution, the confusion due to other sources in the beam can make even the meaning of background dubious. For these reasons we did not subtract the background from the on-source spectra. The large spread of the colours in our diagram is probably the consequence of this choice, as we discuss in the next section.

The colour $[\lambda_i - \lambda_j]$ is defined as:

$$[\lambda_i - \lambda_j] = \log \frac{F_j}{F_i},$$

$F_{i,j}$ being the flux densities in Jy, averaged over a certain band, at the wavelengths $\lambda_{i,j}$. In the case of photometric data, λ is the effective wavelength of the adopted band. Dealing with spectra the choice of the wavelength is somewhat arbitrary. A natural choice is to measure the flux at 60 and 100 μm, which allows a comparison with *IRAS* data. As a third wavelength we adopted 170 μm: this choice was first motivated by the instrumental characteristics of the LWS (as discussed in Tommasi & Pezzuto 1997). It then turned out that these three wavelengths are close to the effective wavelengths of the broadband filters of PACS (Poglitsch, Waelkens & Geis 2002), a far-infrared camera for imaging and spectroscopy which is part of the payload of the future ESA cornerstone mission, the *Herschel Space Observatory*. In such a way it will be possible to use our two-colour diagram with PACS data.

For the bandwidths there is no obvious choice. At first sight a good solution could be to simulate the spectral response of the *IRAS* bands, as the ISAP package allows. There are, however, at least two reasons for not following this approach. The first one is that this choice is not applicable to the third band since *IRAS* did not observe at 170 μm. Secondly, future space missions will enlarge the number of known YSOs, so it is important that our tool does not depend on the photometric bands adopted in previous observations. So, we simply averaged the spectra over 1 μm around the three wavelengths, and verified that our conclusion are not altered when data derived with a completely different instrument, in particular with *IRAS*, are used. This topic will be addressed in the next section.

The uncertainty of the LWS fluxes can be as low as 10 per cent for on-axis, not too-bright nor too-faint, point sources. These conditions are seldom met for our sources, so we adopted a more conservative error of 30 per cent, which turns into an error on each colour of 0.26.

3 RESULTS AND DISCUSSION

In Table 1 we report, for each object: its name; the identifier in the *IRAS* Point Source Catalogue, if present; the LWS and, if available, the *IRAS* colour [60−100]; and the LWS [100−170] colour. The membership of each source to a class has been assessed by looking at the literature.

The [60−100] versus [100−170] diagram is shown in Fig. 1. For comparison we reported the colours, computed following the same procedure outlined before, of a blackbody at various temperatures (marked by crosses and connected by the solid line) ranging from 25 K (top right) to 90 K (bottom left).

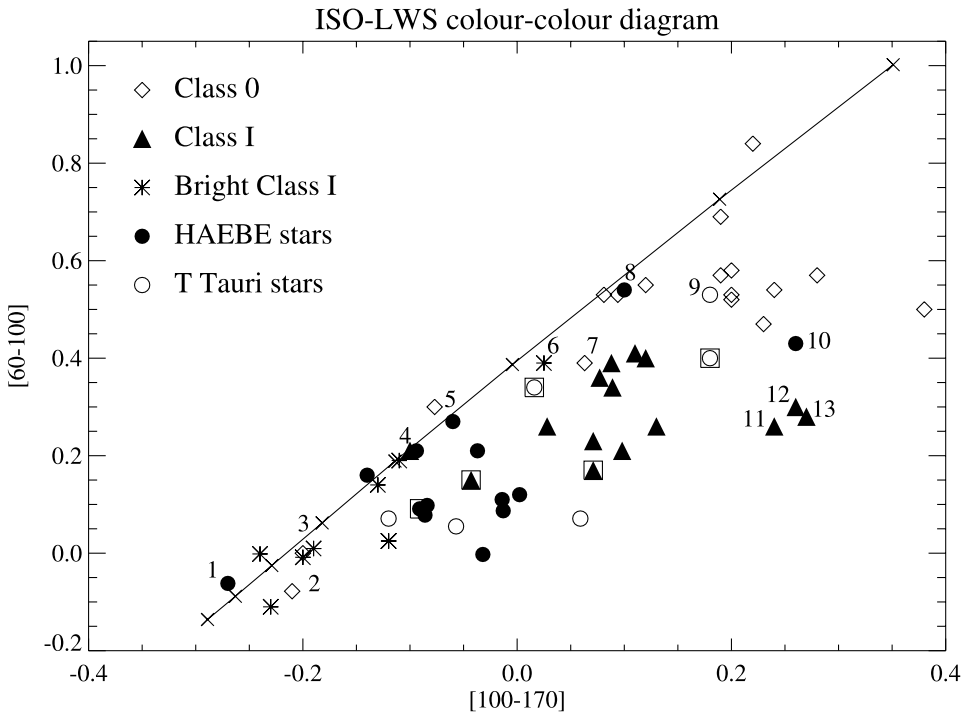

Figure 1. Two-colour diagram for the sample of YSOs. Bright Class I sources are those with bolometric luminosity $L_{bol} > 10^4$ $L_\odot$. Boxed symbols identify FU Orionis objects. The error, not displayed, on each point is 0.26 in both colours, assuming an uncertainty on the fluxes of 30 per cent. Solid line: blackbody colours at temperatures (marked by crosses): 25 K (upper right corner), 30, 40, 50, 60, 70, 80 and 90 K (lower left corner). The numbers identify sources that are individually discussed in the text: (1) MWC 297; (2) FIR 5 and (3) FIR 3 (both in NGC 2024); (4) L 1206; (5) IRAS 2 (in NGC 1333); (6) NGC 281 W; (7) IRAS 18148−0440; (8) IRAS 13547−3944; (9) SR 9; (10) T CrA; (11) IRS 44 and (12) IRS 43 (both in ρ Oph); (13) HH 26 IRS.

The FU Orionis sources are reported in the figure but not considered in the following discussion since their colours are probably influenced by the outbursts of their disc, which represent transient phenomena in the process of star formation.

The sources do not strictly follow the blackbody line, but there is a clear trend of increasing colour temperature T_c with the age of the sources: Class 0 objects have $T_c \sim 30$ K, Class I have $T_c \sim 35-40$ K and for Class II $T_c \sim 50$ K. Bright Class I show the highest temperatures with $T_c \sim 50-80$ K. This trend can be qualitatively explained by considering that at these wavelengths T_c depends only on the temperature stratification of the circumstellar matter. In the first stage of the evolution we can see only the outer region of the envelope at cold temperatures. The optical depth of the envelope decreases with age so that we can look deeper into the inner, and warmer, regions of the envelope and, consequently, T_c increases.

The remainder of this section is organized as follows: first we discuss each class separately and argue that the presence of outlyers, evident in the diagram, can be tentatively explained, in many cases, as due to background contamination. For this reason we cannot average all the colours for each class because this procedure assumes that the dispersion of the points is caused only by random fluctuactions. Instead, we preferred to compute the median, which is less sensitive than the mean to the outlyers. Then, in Section 3.4, we test our result with a different data set, using *IRAS* fluxes, to verify that we did not introduce any bias in the data analysis, at least for the [60−100] colour. Finally, the medians are reported in Fig. 2 along with their root mean square (rms) errors, and their position with respect to the blackbody colours is discussed in Section 3.5.

3.1 Class 0 sources

Class 0 sources appear well clustered in the upper right region of the diagram with [60−100] $\gtrsim 0.45$ and [100−170] $\gtrsim 0.08$, except four objects discussed below. The median colours are: [60−100] $= 0.53 \pm 0.23$ and [100−170] $= 0.19 \pm 0.18$.

IRAS 18148−0440 (number 7 in Fig. 1) has a smaller [100−170] colour and falls closer to Class I sources. It is reported as a Class 0 in the compilation by André, Ward-Thompson & Barsony (2000) but Tafalla et al. (2000) argue that this source is already in a transition state between Class 0 and I. From our diagram we suggest that IRAS 18148 would be better classified as Class I.

The two sources FIR 3 and FIR 5 in NGC 2024 (numbers 2 and 3 in the figure) have blue colours, similar to those of Bright Class I ($L_{bol} > 10^4$ L$_\odot$). From the analysis of the same spectra used in our work, Giannini et al. (2000) have shown that in NGC 2024 the emission lines are mainly produced by the extended cloud in which the sources are embedded. Since the H II region associated with NGC 2024 has a luminosity of 2.8×10^4 L$_\odot$ (Mezger et al. 1992), while for FIR 5 Wiesemeyer et al. (1997) estimate $L_{bol} \sim 1-4$ L$_\odot$, from the position of the sources in our diagram we suggest that the observed continua are dominated by the diffuse PDR more than by the objects themselves.

The source IRAS 2 in NGC 1333 (labelled 5 in the plot) falls close to Class II objects. The *IRAS* colour found by Jennings et al. (1987) and reported in Table 1 is redder than ours and puts the source closer to other Class 0 objects. The fluxes were measured with the Chopped Photometric Channel of *IRAS* which provided a higher angular resolution than that specific to the *IRAS* survey, but it is worth noting that the colour directly measured by *IRAS* is 0.35,

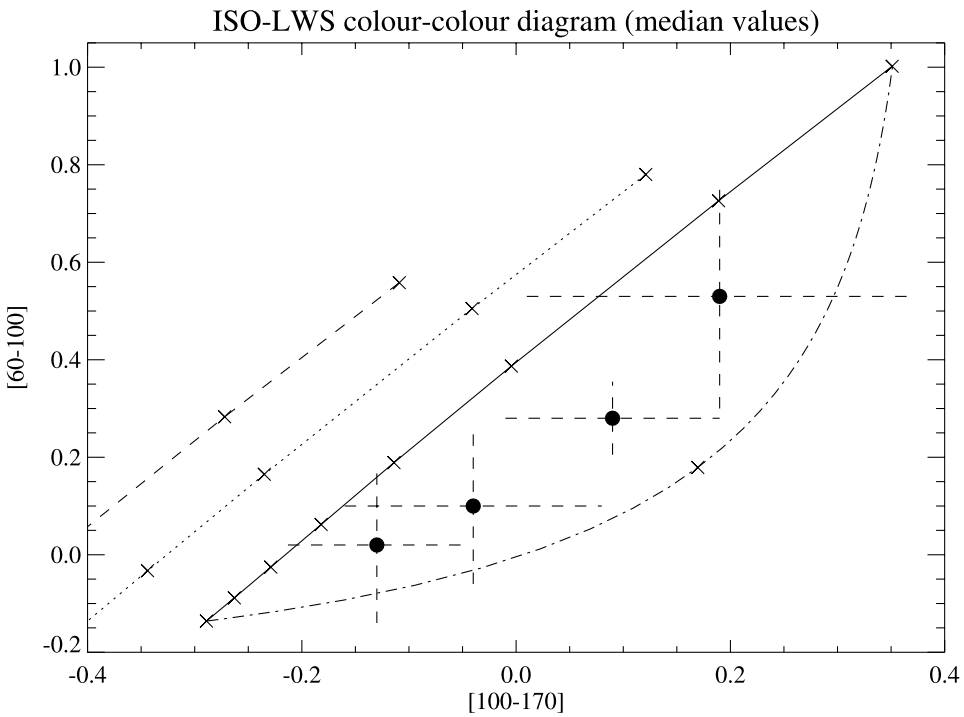

Figure 2. The median colours for each class (filled symbols) with their root-mean-square errors (dashed lines). From top to bottom: Class 0, Class I, Class II and Bright Class I. Solid line: colours of a single blackbody as in Fig. 1; dotted line: colours of a blackbody modified with an emissivity law $\propto \lambda^{-1}$ at T: 25, 30, 40, 50 K; dashed line: as before but with the emissivity $\propto \lambda^{-2}$ and T: 25, 30 K. Dotted–dashed line: colours of two blackbodies at 25 and 90 K and different radii; the cross marks the colours corresponding to the case when the radius of the colder source is 10 times larger than the radius of the warmer source.

not very different from our value of 0.30. It is then probable that the colour we found is strongly affected by the low spatial resolution of the LWS rather than depending on intrinsic characteristics of the source.

3.2 Class I and Bright Class I sources

Without considering the two FU Ori sources, we find for Class I objects the following median colours: $[60-100] = 0.280 \pm 0.075$ and $[100-170] = 0.09 \pm 0.10$. The large scatter in the [100–170] colour is due to the position of L 1206 (source number 4) close to the Class II objects, and to a little 'cluster' of three sources with $[100-170] > 0.2$: for IRS 43 and 44 (numbers 12 and 11 in the figure) the large [100–170] colour is due to the diffuse emission in the ρ Oph complex in which they are embedded. In fact, the subtraction of the background moves their colours into the Class I region.

Objects having a total luminosity $L \geq 10^4\,L_\odot$ have been considered as a distinct group (Bright Class I), since such a high luminosity is usually associated with very-massive hot young stars whose FIR colours are expected to be different from those of lower-luminosity Class I sources. In fact, with the exception of NGC 281W (number 6), they have $[60-170] < 0.2$ and $[100-170] < -0.1$, and fall close to the blackbody line with colour temperatures $T \geq 50\,K$. The median colours are $[60-100] = 0.02 \pm 0.16$ and $[100-170] = -0.130 \pm 0.083$.

The colours of NGC 281W, whose total luminosity is $2.4 \times 10^4\,L_\odot$ (Carpenter, Snell & Schloerb 1990), are the reddest of this group and are in strong disagreement with those of the other objects. We do not have any explanation for such a position.

3.3 Class II sources

This group is divided into low-mass stars, $M \lesssim 2\,M_\odot$, called T Tauri after their prototype, and intermediate-mass stars, $2\,M_\odot \lesssim M \lesssim 8\,M_\odot$, called Herbig Ae/Be stars (or HAEBE). This division reflects physical and observational differences between them, but in our diagram they occupy the same region so, to increase the statistical significance of our work, we will discuss them together. All the Class II objects, with the exception of MWC 297, IRAS 13547, T CrA and SR 9, cluster in a well-defined region of the plot. The median colours of all sources, except the FU Ori, are $[60-100] = 0.11 \pm 0.14$ and $[100-170] = -0.03 \pm 0.12$, with a colour temperature $T_c \sim 50\,K$.

For SR 9 (number 10 in the figure) the fluxes in the on-source position are equal to those in two observed off-source positions so that we conclude that the continuum emission of this T Tauri star is completely dominated by the intense diffuse background of the ρ Oph region, in which SR 9 is embedded, with colours in agreement with those of Class 0 sources (see Table 1). Its [100–170] colour is similar to that of IRS 43 and 44, which also lie in the same region (see the previous discussion).

The anomalous position of the HAEBE star MWC 297, in the bottom left corner and labelled with 1, is compatible with the finding of Drew et al. (1997) that it could be in a more evolved stage and already on the main sequence. In the opposite corner, IRAS 13547 (number 8) and T CrA (10) have colours compatible with Class 0 sources: even if their membership to HAEBE is doubtful, the former being defined as 'potential candidates' and the latter reported among 'other early type emission line stars with IR excess' in the compilation of HAEBE by Thé, de Winter & Pérez (1984), these sources are optically visible and they cannot belong to the group of Class 0. The only conclusion that we can draw from our diagram is that the FIR emission is either produced by a diffuse background, for T CrA see the FIR maps of Wilking et al. (1985), or by a close cold companion.

Table 2. Comparison between median [60–100] colours derived with LWS and *IRAS* data.

	LWS	*IRAS*
Class 0	0.53 ± 0.23	0.53 ± 0.16
Class I	0.280 ± 0.075	0.385 ± 0.078
Bright Class I	0.02 ± 0.16	0.13 ± 0.16
Class II	0.11 ± 0.14	0.12 ± 0.20

3.4 Comparison with *IRAS* data

As we have already pointed out, it is important that the result of our work, i.e. that the [60–100] versus [100–170] diagram is able to separate YSOs belonging to different evolutionary stages, is independent of the instrument used and on the adopted photometric bands. Further, since we neglected instrumental effects, did not take into account the background contamination, defined two colours chosing three arbitrary wavelengths and averaging the fluxes over three arbitrary bandwidths, the reader could wonder about the reproducibility of our finding with different instrument/sample/data analysis.

To address some of these points we compared the median of the [60–100] colours we found with the medians derived using the *IRAS* fluxes, when available in literature. These two sets of data have in common only the effective wavelengths: bandwidths and data acquisition/reduction are completely different. As in our original sample, we did not consider FU Orionis objects. The two sets of medians are reported in Table 2.

For Bright Class I objects, the number of sources with *IRAS* data is too small to draw any conclusion. For Class 0 and II objects, the agreement between the two sets of data is excellent. Only for Class I is the difference larger than 1 rms. From our point of view, however, the difference between 0.280 and 0.385 does not make a big difference in the conclusion that Class I sources occupy a specific region of the diagram. What this difference means is just that we cannot specify with great accuracy what the median [60–100] colour is.

3.5 The median colours: dust emissivity versus source confusion

The median colours are reported in Fig. 2. In this figure we also plotted, as in Fig. 1, the colours of a single blackbody at different temperatures (solid line). In order to clarify why the YSOs have colours under this curve we also plotted the colours of a blackbody modified by an emissivity law $\propto \lambda^{-\beta}$, which better approximates the emission properties of the dust – the main emitter in the FIR. The dashed line corresponds to the case $\beta = 2$, typical of interstellar dust, while the dotted line ($\beta = 1$) is more representative of the dust in the star-forming regions. It is clear from the figure that no positive β can account for the positions of the median values.

Another possible explanation is related to the confusion of the sources inside the LWS beam. It is not possible to model this effect since we should know, object by object, the physical properties and the spatial distribution of the sources around the observed position.

However, we can at least check if this hypothesis moves the colours in the region of the plot where their medians lie, by simply summing the fluxes of two blackbodies. In this case there are three free parameters: the two temperatures and the ratio of their radii. As an example, we have plotted in Fig. 2, the dotted–dashed line, the colours obtained for the temperatures 25 and 90 K, with a ratio varying from 0 to ∞ (the cross symbol marks the case corresponding to the radius of the colder body 10 times larger than the radius of the warmer one). As can be seen, the sum moves the colours in the wanted direction.

The effects of a finite optical depth of the circumstellar envelope, while they cannot be accounted for by a sum of blackbodies, should however be in qualitative agreement with the previous model, so that we can expect also for isolated objects a displacement from the blackbody colours as observed in our plot.

4 CONCLUSIONS

The [60–100] versus [100–170] two-colour diagram has been presented for a sample of YSOs observed with the LWS instrument on-board *ISO*. Each class of YSOs occupies different regions of the diagram with bluer colours corresponding to older classes. The median values of the colours are as follows.

Class 0 : $[60-100] = 0.53 \pm 0.23$
$[100-170] = 0.19 \pm 0.18$

Class I : $[60-100] = 0.280 \pm 0.075$
$[100-170] = 0.09 \pm 0.10$

Bright Class I : $[60-100] = 0.02 \pm 0.16$
$[100-170] = -0.130 \pm 0.083$

Class II : $[60-100] = 0.11 \pm 0.14$
$[100-170] = -0.04 \pm 0.12$

The relative position of the different classes is related to the physical properties of the circumstellar matter and is not an artefact of our data analysis. This has been tested, for the [60–100] colour, through a comparison with *IRAS* data which also show this segregation effect. It is not possible to make such a test for the other colour. However, it is very unlikely that the class separation is due to a bias either in the sample selection or in the data analysis. The change of the colours is a genuine evolutionary effect: in the younger objects we can only observe the outer, and colder, regions of the dusty envelope. The median colours are systematically under the curve of the blackbody colours, and the values we found are probably biased by the combination of both the background contamination and the confusion of the observed sources in the LWS beam. The low spatial resolution of the instrument is indeed the main limitation of our result.

In this respect this work will be greatly improved by future space missions, which will observe with a higher spatial resolution. For instance, the multiband photometric surveys of the FIR camera PACS at ∼60, 100 and 170 μm will be able to make the census of each different evolutionary class of protostellar and pre-main sequence objects in the most important star-forming molecular clouds.

In spite of the present limitation, we conclude that this two-colour diagram offers a powerful and simple tool for the evolutionary classification of YSOs. The advantage over other methods is that follow-up at other wavelengths to identify the evolutionary status will not be needed. As an example, even if we stress that with the LWS data our diagram works mainly as a statistical tool, with only three fluxes and no other photometric measurement it is possible to assign the evolutionary class to the source IRAS 18148−0440: Class I, in agreement with Tafalla et al. (2000), rather than Class 0 (André et al. 2000).

ACKNOWLEDGMENTS

ISO is an ESA project with instruments funded by ESA Member States (especially the Principal Investigator countries: France, Germany, the Netherlands and the United Kingdom) and with the participation of ISAS and NASA.

This research has made use of the SIMBAD data base, operated at CDS, Strasbourg, France. The *ISO* Spectral Analysis Package (ISAP) is a joint development by the LWS and SWS Instrument Teams and Data Centres. Contributing institutes are CESR, IAS, IPAC, MPE, RAL and SRON. LIA is a joint developement of the *ISO*-LWS Instrument Team at Rutherford Appleton Laboratories (RAL, UK – the PI Institute) and the Infrared Processing and Analysis Center (IPAC/Caltech, USA).

We thank an anonymous referee for valuable comments and remarks that significantly improved the manuscript, and we acknowledge fruitful discussions with C. Codella and S. Molinari.

REFERENCES

Adams F. C., Lada C. J., Shu F. H., 1987, ApJ, 312, 788
André P., Ward-Thompson D., Barsony M., 2000, in Mannings V., Boss A. P., Russell S. S., eds, Protostars and Planets IV. Univ. Arizona Press, Tucson, p. 59
Barsony M., Ward-Thompson D., André P., O'Linger J., 1998, ApJ, 509, 733
Beichman C. A., Myers P. C., Emerson J. P., Harris S., Mathieu R., Benson P. J., Jennings R. E., 1986, ApJ, 307, 337
Berrilli F., Ceccarelli C., Liseau R., Lorenzetti D., Saraceno P., Spinoglio L., 1989, MNRAS, 237, 1
Carpenter J. M., Snell R. L., Schloerb F. P., 1990, ApJ, 362, 147
Chen H., Myers P. C., Ladd E. F., Wood D. O. S., 1995, ApJ, 445, 377
Chini R., Kreysa E., Mezger P. G., Gemund H. P., 1986, A&A, 154, L8
Clegg P. E. et al., 1996, A&A, 315, L38
Drew J. E., Busfield G., Hoare M. G., Murdoch K. A., Nixon C. A., Oudmaijer R. D., 1997, MNRAS, 286, 538
Eiroa C., Palacios J., Casali M. M., 1998, A&A, 335, 243
Giannini T. et al., 2000, A&A, 358, 310
Grillo F., 2001, Degree thesis, Università La Sapienza di Roma
Gry C. et al., 2001, The *ISO* Handbook Vol. IV (LWS), SAI-99-077/Dc, Version 1.2. Available online at http://www.iso.vilspa.esa.es/manuals/HANDBOOK/IV/lws_hb/
Hillenbrand L. A., Strom S. E., Vrba F. J., Keene J., 1992, ApJ, 397, 613
Hilton J., White G. J., Cronin N. J., Rainey R., 1986, A&A, 154, 274
Hurt R. L., Barsony M., 1996, ApJ, 460, L45
Jennings R. E., Cameron D. H. M., Cudlip W., Hirst C. J., 1987, MNRAS, 226, 461
Kessler M. et al., 1996, A&A, 315, L27
Leeks S. J., 2000, PhD thesis, Queen Mary & Westfield College, Univ. London
Leeks S. J., Swinyard B. M., Lim T. L., Clegg P. E., 1999, in Cox P., Demuyt V., Kessler M., eds, ESA-SP 427, The Universe as seen by *ISO*. ESA Publications Division, Noordwijk, p. 81

Mezger P. G., Sievers A. W., Haslam C. G. T., Kreysa E., Lemke R., Mauersberger R., Wilson T. L., 1992, A&A, 256, 631
Mookerjea B., Ghosh S. K., Rengarajan T. N., Tandon S. N., Verma R. P., 2000, ApJ, 539, 775
Myers P. C., Ladd E. F., 1993, ApJ, 413, L47
Pezzuto S. et al., 1999, in Cox P., Demuyt V., Kessler M., eds, ESA-SP 427, The Universe as seen by *ISO*. ESA Publications Division, Noordwijk, p. 509
Poglitsch A., Waelkens C., Geis N., 2001, in Pilbratt G. L., Cernicharo J., Heras A. M., Prusti T., Harris R., eds, ESA-SP 460, The Promise of the Herschel Space Observatory. ESA Publications Division, Noordwijk, p. 29
Prusti T., Bontekoe Tj. R., Chiar J. E., Kester D. J. M., Whittet D. C. B., 1993, A&A, 279, 163
Saraceno P., André P., Ceccarelli C., Griffin M., Molinari S., 1996, A&A, 309, 827
Tafalla M., Myers P. C., Mardones D., Bachiller R., 2000, A&A, 359, 967
Thé P. S., de Winter D., Pérez M. R., 1994, A&AS, 104, 315
Tommasi E., Pezzuto S., 1997, in Heras A. M., Leech K., Trams N. R., Perry M., eds, ESA-SP 419, First *ISO* Workshop on Analytical Spectroscopy. ESA Publications Division, Noordwijk, p. 301
White G. J., 1993, A&A, 274, L33
Wiesemeyer H., Güsten R., Wink J. E., Yorke H. W., 1997, A&A, 320, 287
Wilking B. A., Harvey P. M., Joy M., Hyland A. R., Jones T. J., 1985, ApJ, 293, 165
Young E. T., Lada C. J., Wilking B. A., 1986, ApJ, 304, L45

This paper has been typeset from a TEX/LATEX file prepared by the author.